Journal of Alloys and Compounds 1011 (2025) 178480

Contents lists available at ScienceDirect

Journal of Alloys and Compounds

journal homepage: www.elsevier.com/locate/jalcom

Viscosity and crystallization of equiatomic $Pd_{20}Pt_{20}Cu_{20}Ni_{20}P_{20}$ metallic glass

Kalyan Nandigama, Golden Kumar *

Department of Mechanical Engineering, The University of Texas at Dallas, Richardson, TX 75080, USA

ARTICLE INFO

Keywords:
Metallic glass
High entropy
Thermoplastic forming
Fragility

ABSTRACT

Equiatomic metallic glasses are expected to show different properties compared to one principal element-based metallic glasses due to different configurational entropy and atomic-level order. Here, we compare the rheological and transport properties of the supercooled liquid states of compositionally related equiatomic $Pd_{20}Pt_{20}Cu_{20}Ni_{20}P_{20}$ and Pt-rich $Pt_{57.3}Cu_{14.6}Ni_{5.3}P_{22.8}$ metallic glasses. The temperature dependent viscosity values were calculated from thermoplastic molding experiments. The kinetic fragility and isothermal crystallization times were compared to evaluate the correlation between the viscous flow and the diffusivity. The equiatomic metallic glass exhibits stronger liquid behavior, but faster crystallization kinetics than Pt-based metallic glass. The thermoplastic formability of two metallic glasses at different length scales was evaluated using molding and drawing experiments.

1. Introduction

High-entropy alloys (HEAs) and metallic glasses (MGs) are distinct alloy systems with unique structure and properties. HEAs are solid solutions of five or more elements with nearly equiatomic composition [1–3]. Solid solutions stabilized through high configurational entropy or lower enthalpy can enhance the strength of HEAs without reducing the ductility [4–6]. Significant research efforts have been focused on understanding the structure-property correlation in HEAs and on developing new alloys with functional properties [7–9]. In contrast, MGs are typically based on one principal element, and their composition is tailored to increase the glass forming ability by suppressing the competing crystalline phases [10–12].

Conventional MGs become extremely brittle upon crystallization due to the formation of complex intermetallic compounds [13–16]. Recent studies inspired by HEAs have investigated glass formation in equiatomic compositions to potentially benefit from a ductile solid solution phase in the event of crystallization [17–21]. The glass formation, crystallization, and properties of MGs are susceptible to their composition due to atomic-level changes in short-range and medium-range orders [22–24]. Therefore, equiatomic metallic glasses (EA-MGs) are expected to show different properties than single element-based MGs [25]. Zhang *et al.* reported strain hardening and tensile ductility in $Ti_{25}Zr_{25}Hf_{25}Co_{25}$ MG induced by structural ordering whereas typical Zr-based and Ti-based MGs undergo strain softening resulting in catastrophic failure [26].

Several nearly equiatomic glass forming compositions have also been developed to optimize the glass forming ability while retaining the high-entropy characteristics [17,19,20]. Luan *et al.* reviewed the glass formation, the thermal stability, and the mechanical properties of EA-MGs [27]. The glass forming ability of an alloy is inherently linked to the diffusion and viscosity of the supercooled liquid state [11,28,29]. Entropy can affect the diffusion and rheological properties of MGs, but significant configurational entropy enhancement is not expected in MGs because the preferred short-range and medium-range orders can limit the entropic effect. Diffusion kinetics in crystalline HEAs are known to be sluggish due to fluctuation in lattice potential energy [30]. It remains unknown if the deeply undercooled liquid state of HEAs also exhibits slower diffusion which can facilitate glass formation by suppressing crystalline phases. However, high entropy can also reduce liquid viscosity according to the Adam-Gibbs model [31], hindering glass formation. Therefore, it is important to characterize the crystallization and viscosity of equiatomic compositions to understand their glass forming ability. Crystallization and viscosity of supercooled liquids are also important for thermoplastic forming operations. There are limited studies on the viscosity of EA-MGs due to experimental challenges with measuring high viscosity values [32,33]. Typically, dynamic mechanical analysis (DMA) or 3-point bending test is used for the viscosity

* Corresponding author.
E-mail address: golden.kumar@utdallas.edu (G. Kumar).

https://doi.org/10.1016/j.jallcom.2025.178480
Received 13 November 2024; Received in revised form 18 December 2024; Accepted 3 January 2025
Available online 3 January 2025

measurement of metallic glasses [29,34]. However, such methods require thick rectangular beams, which are unattainable from metallic glasses with marginal glass forming ability. In contrast, thermoplastic forming can be used for small samples or irregular shapes and the resulting viscosity values are comparable with other techniques [35,36]. This study uses thermoplastic molding to extract isothermal viscosity values for compositionally related equiatomic $Pd_{20}Pt_{20}Cu_{20}Ni_{20}P_{20}$ (EA-MG) and Pt-rich $Pt_{57.3}Cu_{14.6}Ni_{5.3}P_{22.8}$ (Pt-MG) MGs. Theoretical entropies of mixing for Pt-MG and EA-MG are 1.09 k_B and 1.61 k_B, respectively. The temperature dependent viscosity and crystallization times are compared to understand the correlation between atomic transport and viscous flow.

2. Materials and methods

Crystalline ingots of $Pd_{20}Pt_{20}Cu_{20}Ni_{20}P_{20}$ (EA-MG) and $Pt_{57.3}Cu_{14.6}Ni_{5.3}P_{22.8}$ (Pt-MG) were prepared by melting the elements with purity of 99.9 % or better in vacuum-sealed quartz tubes. The ingots were fluxed with B_2O_3 at 1000 °C to improve the glass forming ability. Small pieces from the fluxed ingots were remelted in thin wall quartz tubes and quenched in water to prepare cylindrical glassy samples of diameters ~ 2 mm. The samples were characterized by a TA Instruments 25 P Differential Scanning Calorimeter (DSC). The glass transition and the crystallization temperatures were compared with the literature values to validate the glassy state of the specimens. The crystallization times and the kinetic fragility were calculated from the isothermal and constant heating rate DSC curves, respectively.

The samples were thermoplastically molded against silicon templates consisting of 10 μm diameter cylindrical cavities. The molding experiments were performed at different temperatures above the glass transition by ramping the load to 500 N in 60 s. A custom-made thermomechanical molding setup was used whose details are described in our previous work [36,37]. The silicon was etched away in KOH and the MG micro-pillars were characterized by a Zeiss Supra 40 scanning electron microscope (SEM). The supercooled liquid viscosity was extracted from the lengths of micro-pillars using the previous model for thermoplastic forming [38]. The lengths of multiple pillars at different locations were used to calculate the average viscosity values and the error bars. Additional error in viscosity values due to the measurement of pillar lengths was estimated to be less than a factor of 1.3. Nanoporous alumina with 150 nm diameter pores was used as a template to evaluate the nanoscale molding ability of both MGs.

3. Results and discussion

Fig. 1 compares the DSC curves of EA-MG and Pt-MG recorded at a heating rate of 0.33 K/s. The specimens show distinct endothermic and exothermic reactions corresponding to glass transition and crystallization, respectively. The glass transition onset temperature (T_g), crystallization onset temperature (T_x), and the supercooled liquid temperature range ($\Delta T_x = T_x - T_g$) are summarized in Table 1. EA-MG and Pt-MG show a wide ΔT_x range which indicates high glass forming ability and suitability for thermoplastic forming operations. It has been reported that an amorphous sample with a diameter exceeding 10 mm can be prepared for EA-MG alloy [39]. In addition to forming bulk feedstock, thermoplastic processing also requires thermal stability and access to low viscosity of the MG supercooled liquid. The thermoplastic forming potential of Pt-MG has been extensively studied [40–42]. Next, we compare the thermal stability and viscosity of EA-MG with Pt-MG in the supercooled liquid state.

The thermoplastic forming temperature can be determined using isothermal DSC curves by ensuring that the total processing time is kept well below the crystallization time. Fig. 2 presents the isothermal crystallization times for EA-MG and Pt-MG supercooled liquids plotted as a function of temperature normalized by T_g. The overall trend is similar, but the EA-MG shows faster crystallization kinetics at

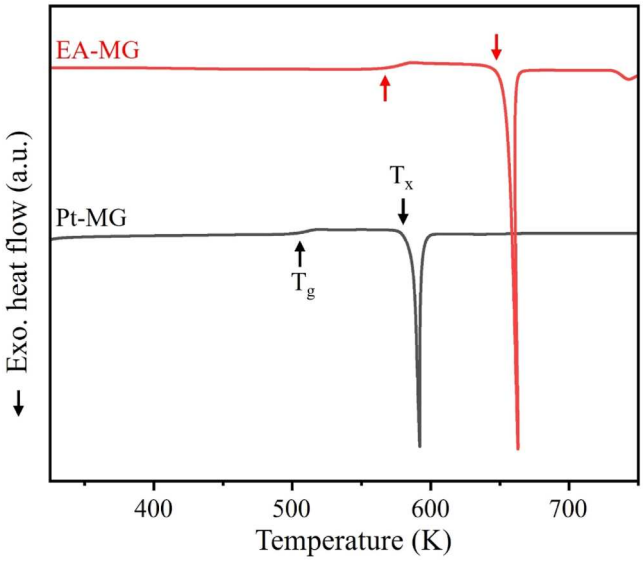

Fig. 1. DSC curves of EA-MG and Pt-MG measured at a heating rate 0.33 K/s. The onset of glass transition and crystallization temperatures are indicated.

Table 1
Thermodynamic properties and VFT parameters of EA-MG and Pt-MG. The error in DSC data is less than ± 2 K.

Metallic glass	T_g (K)	T_x (K)	ΔT_x (K)	T_o (K)	D^*
$Pt_{20}Pd_{20}Cu_{20}Ni_{20}P_{20}$ (EA-MG)	566	645	79	390	15.1
$Pt_{57.3}Cu_{14.6}Ni_{5.3}P_{22.8}$ (Pt-MG)	500	590	90	362[a]	11.8

[a] From Ref. [45].

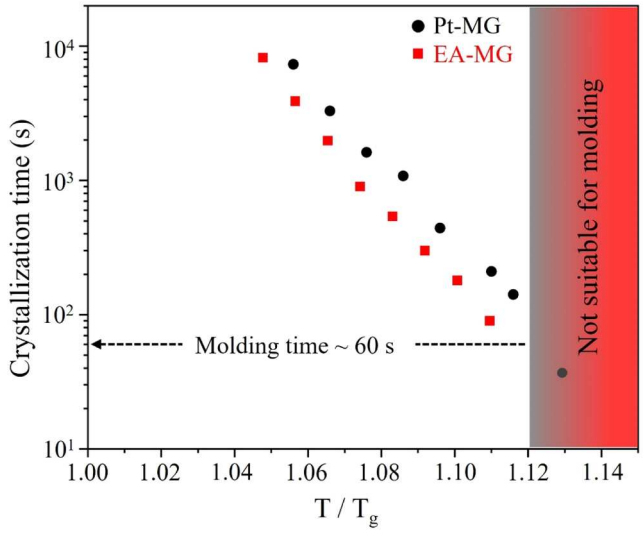

Fig. 2. Isothermal crystallization times of EA-MG and Pt-MG plotted as a function of normalized temperature. The temperature range with a crystallization time shorter than 60 s is marked "not suitable" for thermoplastic molding.

comparable normalized temperatures. The crystallization time at $1.11T_g$ is about 90 s for EA-MG compared to 210 s for Pt-MG. It has been predicted that the maximum thermoplastic deformation of MGs is achieved at the highest possible temperature if crystallization can be avoided during forming operation [43]. A typical molding time of 60 s sets an upper limit of thermoplastic processing temperature of about $1.12T_g$ for both MGs (Fig. 2).

Microscale molding experiments were performed at various temperatures above T_g to evaluate the thermoplastic forming potential of EA-MG. Fig. 3 compares the SEM images of Pt-MG and HE-MG micro-pillars molded at three temperatures. Pt-MG forms micro-pillars with aspect ratios exceeding 3 at a relatively low temperature of $1.05T_g$ (513 K) validating the excellent thermoplastic formability of Pt-MG. In contrast, molding of EA-MG at a higher temperature of $1.08T_g$ (613 K) results in micro-pillars of aspect ratios of about 2. The pillar height increases at higher molding temperatures due to a reduction in viscosity. At the microscale, the length of molded structures is inversely proportional to the viscosity by $\propto 1/\sqrt{viscosity}$ [38,41]. The molding results indicate that the EA-MG supercooled liquid exhibits higher viscous resistance compared to Pt-MG at the same normalized temperatures. The viscosity values were calculated from the pillar dimensions and the loading conditions by using the Newtonian flow model described in previous work [36,38].

Fig. 4 plots the temperature dependent viscosity of two MGs extracted from microscale molding experiments. For EA-MG, the viscosity value was assumed to be 10^{12} Pa·s at the caloric glass transition because the thermoplastic forming was not feasible due to high viscosity. The viscosity of Pt-MG at different temperatures has been previously calculated using thermoplastic forming [38,40] and VFT equation [44]. The current viscosity values are within the range of error, demonstrating the reproducibility of the thermoplastic forming approach. The viscosity of EA-MG supercooled liquid remains at least three orders of magnitude higher than Pt-MG at each normalized temperature. Furthermore, the viscosity of EA-MG shows weaker temperature dependence, which is a characteristic of strong glass-forming liquids. The EA-MG exhibits an Arrhenius behavior whereas a large deviation is observed for fragile Pt-MG. The fragility of supercooled liquids captures the dynamical arrest near T_g which is important for glass forming ability and thermoplastic processing. The higher viscosity of EA-MG suggests that an equiatomic composition does not result in entropy enhancement that would reduce viscosity, according to the Adam-Gibbs model.

The fragility of EA-MG was calculated by measuring the DSC curves at different heating rates and fitting the data with the Vogel–Fulcher–Tamann (VFT) equation. Selected DSC curves at various heating rates are shown in Fig. 5a. The glass transition shifts to higher temperatures with increasing heating rates, but the width of the transition ($\Delta T_g = T_{g\ \text{complete}} - T_{g\ \text{onset}}$) remains nearly constant at about ~

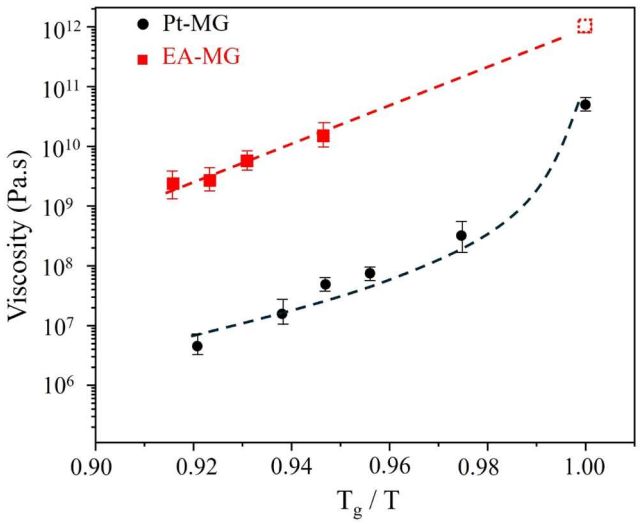

Fig. 4. Temperature dependence of viscosity values for EA-MG and Pt-MG calculated from the molded pillar lengths. The viscosity at calorimetric T_g is assumed to be 10^{12} Pa·s for EA-MG (dotted square symbol).

20 K. The VFT equation for relaxation time, τ_g, at glass transition, can be written as

$$\tau_g = \tau_o \exp\left(\frac{D^*.\ T_0}{T_g - T_0}\right), \quad (1)$$

where τ_o is the infinite temperature relaxation time with a value of about 2×10^{-13} s [31], D^* is the fragility parameter, and T_o is the temperature corresponding to infinite relaxation time. The relaxation time can also be calculated from the width of the glass transition and the heating rate, R_h, as

$$\tau_g = \frac{\Delta T_g}{R_h}, \quad (2)$$

The VFT equation in terms of T_g and heating rate can then be obtained by combining Eqs. (1) and (2) yielding

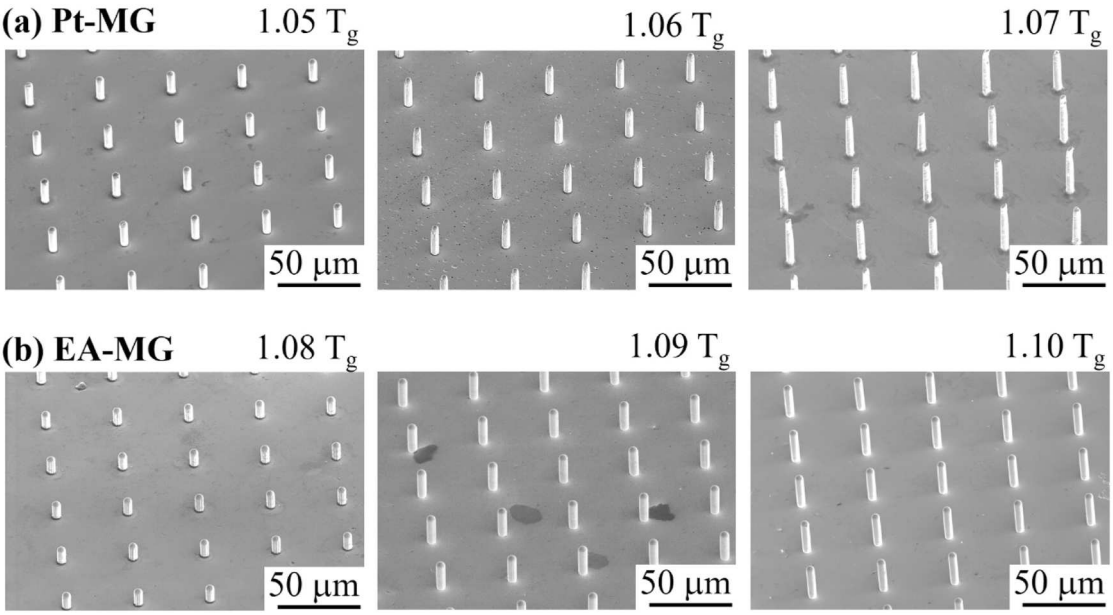

Fig. 3. SEM images of EA-MG and Pt-MG micro-pillars formed by thermoplastic molding at three different temperatures.

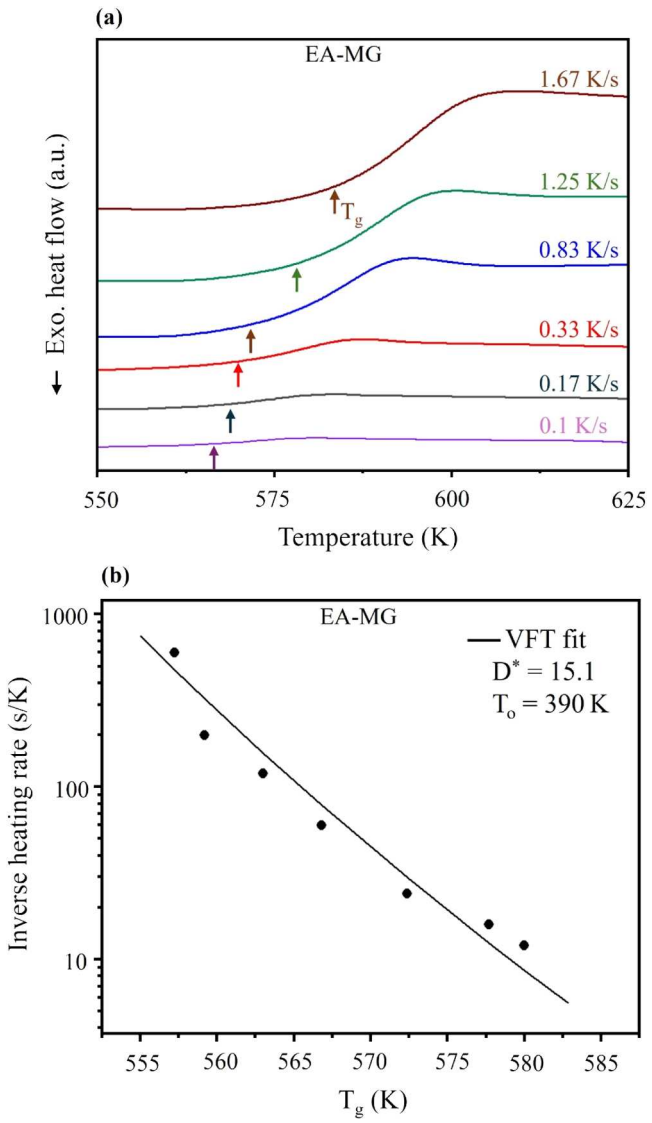

Fig. 5. (a) Glass transition temperature measured at different heating rates in DSC curves. (b) Inverse heating rate as a function of glass transition temperature used for VFT fit. The fitting parameters are listed.

$$\frac{\Delta T_g}{R_h} = \tau_o \exp\left(\frac{D^*.\ T_0}{T_g - T_0}\right), \quad (3)$$

The VFT parameters D^* and T_o can be determined by fitting the heating rate dependent T_g values because ΔT_g and τ_o are constants. In Fig. 5b, the T_g onset values are plotted as a function of inverse heating rate. The solid line shows the best fit to Eq. (3) and the fitting variables D^* and T_o are 15.1 and 390 K, respectively (Table 1). The larger D^* value for EA-MG compared to 11.8 for Pt-MG [45] is consistent with the viscosity data obtained from the molding experiments. The EA-MG supercooled liquid exhibits stronger liquid behavior compared to Pt-MG. The compositional dependence of fragility in glass forming liquids is typically attributed to different atomic structures [45]. The previous study revealed significant differences in short-range and medium-range orders in Pt-Pd-Cu-Ni-P glass-forming alloys with varying Pt and Pd contents [46]. Addition of Pd to Pt-Cu-Ni-P MG promotes formation of icosahedral short-range order [46]. A similar difference in atomic-level order is likely the origin of the different fragility observed for EA-MG and Pt-MG.

The viscous flow and atomic transport in MG supercooled liquids have often been linked by the Stokes-Einstein relation, $D_{\text{eff}} \propto \eta^{-1}$ (D_{eff} is effective diffusivity and η is viscosity). However, the viscosity and crystallization data for both EA-MG and Pt-MG supercooled liquids suggest the decoupling of time scales for viscosity and diffusion. The time to crystallize (t_x) a small volume fraction (x) can be expressed in terms of steady-state nucleation rate (I_s) and growth rate (u) as [47]

$$t_x = \left(\frac{3x}{\pi I_s u^3}\right)^{1/4}, \quad (4)$$

Using expressions for I_s and u, Eq. (4) yields an inverse relationship between t_x and D_{eff}. Therefore, the Stokes-Einstein formulation predicts a proportional relation between t_x and η. However, the experimental results show different temperature dependencies for the time scales for diffusion and viscous flow in both MGs. Accelerated crystallization at all temperatures is observed in EA-MG despite high viscosity. The EA-MG crystallizes into non-isomorphic Ni_3P, PtP_2, Pd_2Ni_2P, and *fcc*-(Pd, Ni) phases which require long-range diffusion [39]. The diffusivity necessary for nucleation and growth of these crystalline phases is achieved regardless of the high viscosity of EA-MG supercooled liquid. Similarly, the low viscosity and long crystallization times for Pt-MG are in contradiction to the Stokes-Einstein relation. The unusual thermal stability of fragile Pt-MG has been explained by the high interfacial energy [44]. Earlier studies have shown fast diffusion of medium sized atoms in deeply supercooled MGs based on a solid-like collective hopping mechanism [48,49]. A similar mechanism is likely responsible for the higher diffusivity of EA-MG. It has been reported that pronounced icosahedral short-range order exists in supercooled liquid state of Pd-Pt-Ni-Cu-P MGs [46]. This can also explain the absence of entropy enhancement and higher viscosity of EA-MG supercooled liquid. High viscosity has also been reported in equiatomic Ti-Zr-Hf-Ni-Cu-Be MG [32].

The high viscosity and low fragility of MG supercooled liquids make their thermoplastic forming operations difficult. The forming challenge exacerbates for nanoscale structures with high aspect ratios which require impractical molding pressure for high viscosity liquids. Fig. 6 shows the SEM images of Pt-MG and EA-MG molded against 150 nm diameter nanoporous alumina. The molding was performed by applying 150 MPa pressure for 180 s at 40 K and 50 K above T_g for Pt-MG and EA-MG, respectively. EA-MG forms short nanorods with aspect ratios of only 2–3 whereas Pt-MG nanorods exceed an aspect ratio of 10. The difference in lengths of nanorods for two MGs is due to their different viscosities. Large aspect ratio nanorods in high viscosity EA-MG require a molding pressure approaching several gigapascals which exceeds the strength of the molds.

Thermoplastic drawing has been reported to be advantageous for fabrication of very high aspect ratio structures because of low pressure requirements due to the absence of mold friction [37,50]. Fig. 6 shows the MG nanowires drawn at 20 mm/min from silicon molds after pressing under 25 MPa at the same temperatures as the nanoscale molding. The drawing results in the formation of long EA-MG nanowires despite three orders of magnitude higher viscosity. The profiles of drawn nanowires are similar in both MGs indicating an overall similar flow behavior. Therefore, thermoplastic drawing is better suited for high viscosity MGs such as EA-MG.

4. Conclusions

In summary, the isothermal viscosities and crystallization kinetics of equiatomic $Pd_{20}Pt_{20}Cu_{20}Ni_{20}P_{20}$ and Pt-rich $Pt_{57.3}Cu_{14.6}Ni_{5.3}P_{22.8}$ glass forming alloys were investigated. The viscosity values extracted from the molding experiments showed weaker temperature dependence for the equiatomic alloy. These findings were supported by the VFT data which revealed a higher fragility parameter D^* of 15.1 supporting the stronger liquid behavior of equiatomic metallic glass compared to the Pt-based counterpart. Despite high viscosity, the equiatomic supercooled liquid exhibits faster crystallization kinetics indicating the decoupling of times scale for viscous flow and diffusivity. The high viscosity and short

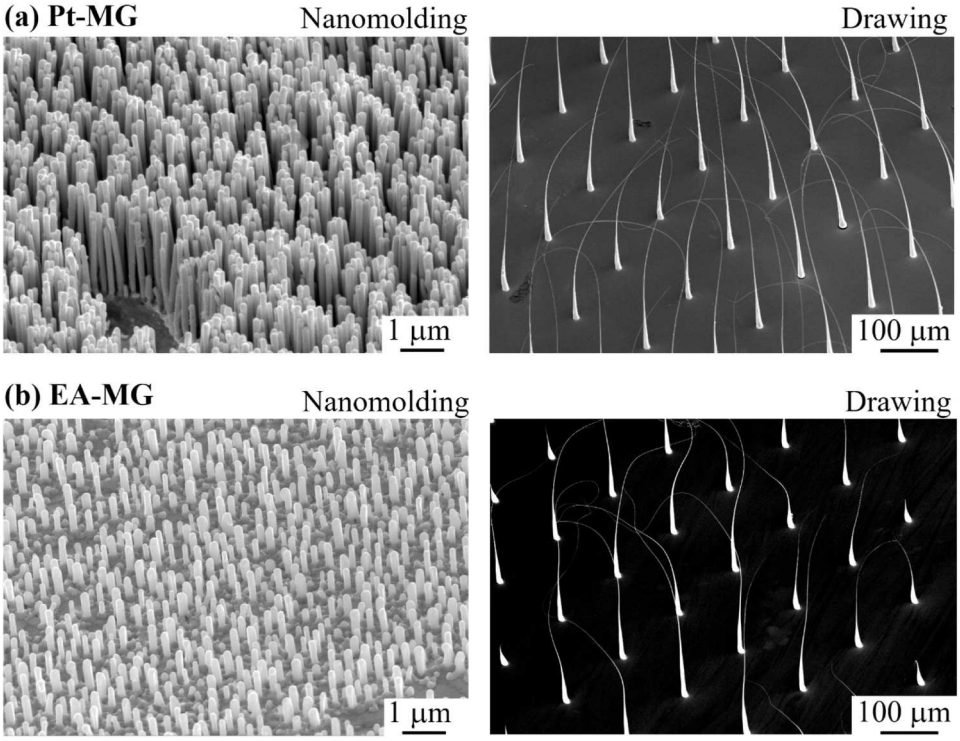

Fig. 6. Comparison of thermoplastic molding and drawing outcomes at the nanoscale for EA-MG and P-MG. The drawing can generate high aspect-ratio nanostructures from MGs with higher viscosities.

crystallization time in equiatomic $Pd_{20}Pt_{20}Cu_{20}Ni_{20}P_{20}$ metallic glass are attributed to the presence of strong short-range order. The results suggest that equiatomic composition may not result in entropy enhancement in metallic glasses. The high viscosity and fast crystallization of equiatomic alloy make thermoplastic molding difficult, but drawing can generate long nanowires.

CRediT authorship contribution statement

Golden Kumar: Writing – review & editing, Supervision, Project administration, Funding acquisition, Conceptualization. **Kalyan Nandigama:** Writing – original draft, Formal analysis, Data curation.

Declaration of Competing Interest

The authors declare that they have no known competing financial interests or personal relationships that could have appeared to influence the work reported in this paper.

Acknowledgements

The work was supported by the US National Science Foundation (NSF) through Award # 2212195.

Data availability

Data will be made available on request.

References

[1] J.W. Yeh, S.K. Chen, S.J. Lin, J.Y. Gan, T.S. Chin, T.T. Shun, C.H. Tsau, S.Y. Chang, Nanostructured high-entropy alloys with multiple principal elements: novel alloy design concepts and outcomes, Adv. Eng. Mater. 6 (2004) 299–303.
[2] Y. Zhang, T.T. Zuo, Z. Tang, M.C. Gao, K.A. Dahmen, P.K. Liaw, Z.P. Lu, Microstructures and properties of high-entropy alloys, Prog. Mater. Sci. 61 (2014) 1–93.
[3] D.B. Miracle, O.N. Senkov, A critical review of high entropy alloys and related concepts, Acta Mater. 122 (2017) 448–511.
[4] Y. Zhang, Y.J. Zhou, J.P. Lin, G.L. Chen, P.K. Liaw, Solid-solution phase formation rules for multi-component alloys, Adv. Eng. Mater. 10 (2008) 534–538.
[5] X. Yang, Y. Zhang, Prediction of high-entropy stabilized solid-solution in multi-component alloys, Mater. Chem. Phys. 132 (2012) 233–238.
[6] E.P. George, D. Raabe, R.O. Ritchie, High-entropy alloys, Nat. Rev. Mater. 4 (2019) 515–534.
[7] O.N. Senkov, G.B. Wilks, D.B. Miracle, C.P. Chuang, P.K. Liaw, Refractory high-entropy alloys, Intermetallics 18 (2010) 1758–1765.
[8] C. Zhang, Q. Yu, Y.B.T. Tang, M.J. Xu, H.R. Wang, C.Y. Zhu, J. Ell, S.T. Zhao, B. E. MacDonald, P.H. Cao, J.M. Schoenung, K.S. Vecchio, R.C. Reed, R.O. Ritchie, E. J. Lavernia, Strong and ductile FeNiCoAl-based high-entropy alloys for cryogenic to elevated temperature multifunctional applications, Acta Mater. 242 (2023) 118449.
[9] J.Y. He, W.H. Liu, H. Wang, Y. Wu, X.J. Liu, T.G. Nieh, Z.P. Lu, Effects of Al addition on structural evolution and tensile properties of the FeCoNiCrMn high-entropy alloy system, Acta Mater. 62 (2014) 105–113.
[10] A. Inoue, Stabilization of metallic supercooled liquid and bulk amorphous alloys, Acta Mater. 48 (2000) 279–306.
[11] W.L. Johnson, Bulk glass-forming metallic alloys: science and technology, Mrs Bull. 24 (1999) 42–56.
[12] W.H. Wang, Roles of minor additions in formation and properties of bulk metallic glasses, Prog. Mater. Sci. 52 (2007) 540–596.
[13] G. Kumar, M. Ohnuma, T. Furubayashi, T. Ohkubo, K. Hono, Thermal embrittlement of Fe-based amorphous ribbons, J. Non-Cryst. Solids 354 (2008) 882–888.
[14] P. Murali, U. Ramamurty, Embrittlement of a bulk metallic glass due to sub-T-g annealing, Acta Mater. 53 (2005) 1467–1478.
[15] G.R. Garrett, M.D. Demetriou, M.E. Launey, W.L. Johnson, Origin of embrittlement in metallic glasses, Proc. Natl. Acad. Sci. USA 113 (2016) 10257–10262.
[16] G. Kumar, D. Rector, R.D. Conner, J. Schroers, Embrittlement of Zr-based bulk metallic glasses, Acta Mater. 57 (2009) 3572–3583.
[17] M.L. Liu, W. Li, S. Zeng, Y.F. Li, H.M. Fu, H. Li, A.M. Wang, X.P. Lin, H.F. Zhang, Z. W. Zhu, Ductilizing Ti19Zr19Hf19Nb19TM5Be19 (TM = Fe, Co, Ni and Cu) high-entropy bulk metallic glass composites via precipitated refractory high-entropy alloy dendrites, Intermetallics 152 (2023) 107755.
[18] S.H. Hong, H.J. Park, G.C. Kang, Y.S. Kim, G. Song, K.B. Kim, Nanocrystalline single-phase high-entropy alloy synthesized by using intermetallic compound type (TiZrHf)-(NiCuCo) high-entropy metallic glass precursor, Scr. Mater. 209 (2022) 114391.
[19] M.C. Li, H.M. Guan, S. Yang, X. Ma, Q. Li, Minor Cr alloyed Fe-Co-Ni-P-B high entropy bulk metallic glass with excellent mechanical properties, Mater. Sci. Eng. A-Struct. Mater. Prop. Microstruct. Process. 805 (2021) 140542.

[20] J. Kim, H.S. Oh, J. Kim, C.W. Ryu, G.W. Lee, H.J. Chang, E.S. Park, Utilization of high entropy alloy characteristics in Er-Gd-Y-Al-Co high entropy bulk metallic glass, Acta Mater. 155 (2018) 350–361.
[21] B.A. Welk, M.A. Gibson, H.L. Fraser, A combinatorial approach to the investigation of metal systems that form both bulk metallic glasses and high entropy alloys, Jom 68 (2016) 1021–1026.
[22] D.B. Miracle, A structural model for metallic glasses, Nat. Mater. 3 (2004) 697–702.
[23] G. Kumar, D. Nagahama, M. Ohnuma, T. Ohkubo, K. Hono, Structural evolution in the supercooled liquid of Zr36Ti24Be40 metallic glass, Scr. Mater. 54 (2006) 801–805.
[24] S.Y. Ding, Y.H. Liu, Y.L. Li, Z. Liu, S. Sohn, F.J. Walker, J. Schroers, Combinatorial development of bulk metallic glasses, Nat. Mater. 13 (2014) 494–500.
[25] X. Zhang, H. Luan, H. Lou, T. Liang, S. Chen, D. Xu, Z. Yin, L. Wang, J. Zeng, Y. Ren, Z. Zeng, Y. Shao, K.F. Yao, Q. Zeng, Highly variable chemical short-range order in a high-entropy metallic glass, Mater. Today Phys. 27 (2022) 100799.
[26] Z.B. Zhang, S. Zhang, Q. Wang, A.L. Lu, Z.Q. Chen, Z.Y. Yang, J.H. Luan, R. Su, P. F. Guan, Y. Yang, Intrinsic tensile ductility in strain hardening multiprincipal element metallic glass, Proc. Natl. Acad. Sci. USA 121 (2024) e2400200121.
[27] H.W. Luan, K.R. Li, L.X. Shi, W. Zhao, H.T. Bu, P. Gong, K.F. Yao, Recent progress in high-entropy metallic glasses, J. Mater. Sci. Technol. 161 (2023) 50–62.
[28] R. Busch, A. Masuhr, E. Bakke, W.L. Johnson, Bulk metallic glass formation from strong liquids, Mech. Alloy. Metastable Nanocrystall. Mater. 2 (269-2) (1998) 547–552.
[29] R. Busch, E. Bakke, W.L. Johnson, Viscosity of the supercooled liquid and relaxation at the glass transition of the Zr46.75Ti8.25Cu7.5Ni10Be27.5 bulk metallic glass forming alloy, Acta Mater. 46 (1998) 4725–4732.
[30] K.Y. Tsai, M.H. Tsai, J.W. Yeh, Sluggish diffusion in Co-Cr-Fe-Mn-Ni high-entropy alloys, Acta Mater. 61 (2013) 4887–4897.
[31] R. Busch, J. Schroers, W.H. Wang, Thermodynamics and kinetics of bulk metallic glass, Mrs Bull. 32 (2007) 620–623.
[32] Y. Tong, J.C. Qiao, J.M. Pelletier, Y. Yao, Strong metallic glass: TiZrHfCuNiBe high entropy alloy, J. Alloy. Compd. 820 (2020) 153119.
[33] X.Y. Wang, W.L. Dai, M. Zhang, P. Gong, N. Li, Thermoplastic micro-formability of TiZrHfNiCuBe high entropy metallic glass, J. Mater. Sci. Technol. 34 (2018) 2006–2013.
[34] J.C. Qiao, S. Cardinal, J.M. Pelletier, H. Kato, Insight on the process ability of bulk metallic glasses by thermo-mechanical analysis and dynamic mechanical analysis, J. Alloy. Compd. 628 (2009) 357–363.
[35] G. Kumar, H.X. Tang, J. Schroers, Nanomoulding with amorphous metals, Nature 457 (2009) 868–872.
[36] A. Jabed, C.S. Meduri, G. Kumar, Effect of time on the isothermal viscosity of metallic glass supercooled liquids, J. Alloy. Compd. 863 (2021) 158067.
[37] S. Jagdale, A. Jabed, S. Theeda, C.S. Meduri, Z.L. Hu, M. Hasan, G. Kumar, Review of thermoplastic drawing with bulk metallic glasses, Metals 12 (2022) 518.
[38] G. Kumar, J. Schroers, J. Blawzdziewicz, Controllable nanoimprinting of metallic glasses: effects of pressure and interfacial properties, Nanotechnology 24 (2013) 105301.
[39] A. Takeuchi, N. Chen, T. Wada, Y. Yokoyama, H. Kato, A. Inoue, J.W. Yeh, PdPtCuNiP high-entropy alloy as a bulk metallic glass in the centimeter, Intermetallics 19 (2011) 1546–1554.
[40] J. Schroers, On the formability of bulk metallic glass in its supercooled liquid state, Acta Mater. 56 (2008) 471–478.
[41] G. Kumar, A. Desai, J. Schroers, Bulk metallic glass: the smaller the better, Adv. Mater. 23 (2011) 461–476.
[42] L. Liu, M. Hasan, G. Kumar, Metallic Glass nanostructures: fabrication, properties, and applications, Nanoscale 6 (2014) 2027–2036-476.
[43] E.B. Pitt, G. Kumar, J. Schroers, Temperature dependence of the thermoplastic formability in bulk metallic glasses, J. Appl. Phys. 110 (2011) 043518.
[44] B.A. Legg, J. Schroers, R. Busch, Thermodynamics, kinetics, and crystallization of Pt57.3Cu14.6Ni5.3P22.8 bulk metallic glass, Acta Mater. 55 (2007) 1109–1116.
[45] I. Gallino, O. Gross, G.D. Fontana, Z. Evenson, R. Busch, On the kinetic and thermodynamic fragility of the PtCuCoP and PtCuNiP bulk metallic glasses, J. Alloy. Compd. 615 (2014) S35–S39.
[46] O. Gross, N. Neuber, A. Kuball, B. Bochtler, S. Hechler, M. Frey, R. Busch, Signatures of structural differences in Pt-P- and Pd-P-based bulk glass-forming liquids, Commun. Phys. 2 (2019) 83.
[47] D.R. Uhlmann, Crystal-Growth in Glass-Forming Systems. Abstracts of Papers of the American Chemical Society (1975) 39-39.
[48] A. Masuhr, T.A. Waniuk, R. Busch, W.L. Johnson, Time scales for viscous flow, atomic transport, and crystallization in the liquid and supercooled liquid states of Zr41.2Ti13.8Cu12.5Ni10.0Be22.5, Phys. Rev. Lett. 82 (1999) 2290–2293.
[49] F. Faupel, W. Frank, M.P. Macht, H. Mehrer, V. N, K. Ratzke, H.R. Schober, S. K. Sharma, H. Teichler, Diffusion in metallic glasses and supercooled melts, Rev. Mod. Phys. 75 (2003) 237–280.
[50] Z. Hu, C.S. Meduri, J. Blawzdziewicz, G. Kumar, Nanoshaping of glass forming metallic liquids by stretching: evading lithography, Nanotechnology 30 (2018) 075302.